ARMY RESEARCH LABORATORY

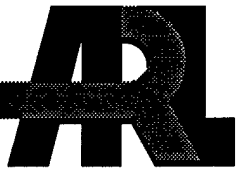

X-Ray Diffraction Characterization of Process-Induced Residual Stress

Daniel J. Snoha

ARL-TR-1204 September 1996

NOTICES

Destroy this report when it is no longer needed. DO NOT return it to the originator.

Additional copies of this report may be obtained from the National Technical Information Service, U.S. Department of Commerce, 5285 Port Royal Road, Springfield, VA 22161.

The findings of this report are not to be construed as an official Department of the Army position, unless so designated by other authorized documents.

The use of trade names or manufacturers' names in this report does not constitute indorsement of any commercial product.

REPORT DOCUMENTATION PAGE

Form Approved
OMB No. 0704-0188

1. AGENCY USE ONLY *(Leave blank)*	2. REPORT DATE	3. REPORT TYPE AND DATES COVERED
	September 1996	Summary, Jan 90 - Dec 94

4. TITLE AND SUBTITLE

X-Ray Diffraction Characterization of Process-Induced Residual Stress

5. FUNDING NUMBERS

N/A

6. AUTHOR(S)

Daniel J. Snoha

7. PERFORMING ORGANIZATION NAME(S) AND ADDRESS(ES)

U.S. Army Research Laboratory
ATTN: AMSRL-MA-I
Aberdeen Proving Ground, MD 21005-5069

8. PERFORMING ORGANIZATION REPORT NUMBER

ARL-TR-1204

9. SPONSORING/MONITORING AGENCY NAMES(S) AND ADDRESS(ES)

10.SPONSORING/MONITORING AGENCY REPORT NUMBER

11. SUPPLEMENTARY NOTES

12a. DISTRIBUTION/AVAILABILITY STATEMENT

Approved for public release; distribution is unlimited.

12b. DISTRIBUTION CODE

13. ABSTRACT *(Maximum 200 words)*

The U.S. Army Research Laboratory - Materials Directorate (ARL-MD) has utilized the x-ray diffraction (XRD) method of residual stress analysis (RSA) to characterize process-induced residual stress on a variety of polycrystalline metal and ceramic materials. As part of the mechanical failure investigation, modern XRD RSA techniques provide a direct means for quantifying residual stress at the component surface - the location at which most fatigue and stress corrosion cracks originate. Therefore, an understanding of the magnitude and distribution of residual stresses introduced from processing is important when predicting failure modes through fracture mechanics calculations and service loads by finite element modeling. This report discusses the procedures for and results from XRD residual stress measurement on the following differently processed material systems: shot-peened stainless steel, quenched and tempered and welded armor steel, autofrettage gun tube steel, and ground alumina ceramic.

14. SUBJECT TERMS

x-ray diffraction, residual stress, shot peen, welding, grinding, autofrettage

15. NUMBER OF PAGES

18

16. PRICE CODE

17. SECURITY CLASSIFICATION OF REPORT	18. SECURITY CLASSIFICATION OF THIS PAGE	19. SECURITY CLASSIFICATION OF ABSTRACT	20. LIMITATION OF ABSTRACT
UNCLASSIFIED	UNCLASSIFIED	UNCLASSIFIED	UL

TABLE OF CONTENTS

LIST OF FIGURES

LIST OF TABLES

1. INTRODUCTION

The nondestructive, noncontact x-ray diffraction (XRD) residual stress analysis technique has found widespread application (Kula and Veiss 1982; ASM International 1991; Hauk, Hougardy, and Macherauch 1991) and is generally accepted as being the most accurate of the experimental methodologies for residual stress determination.[1] XRD residual stress measurement is based upon the fact that strain induced in a crystalline material as a consequence of mechanical deformation, phase transformation, thermal expansion, etc., causes a change in the spacing of the atomic planes within the crystal structure from that in the stress-free condition. This change in interatomic, or d-, spacing is evidenced as a shift in the diffracted x-ray peak position. By resolving the angular peak shift and applying the Bragg law $\eta\lambda = 2d \sin\theta$ (the relation that describes XRD) to quantify the d-spacing, the stress on the surface of the specimen can be calculated via linear elastic theory. Assuming that plane stress conditions exist on the surface (i.e., a biaxial system), the relationship of interatomic strain to stress is given by:

$$\varepsilon_{\phi\psi} = \left[(1+\upsilon)/E\right]\sigma_\phi \sin^2\psi - \upsilon/E\left(\sigma_1+\sigma_2\right), \tag{1}$$

where

$\varepsilon_{\phi\psi} = \left(d_{\phi\psi}-d_0\right)/d_0$ = strain in the direction defined by angles ϕ and ψ (d_0 is the interatomic spacing in the stress-free condition)

E, υ = material elastic constants

σ_ϕ = surface stress in the direction defined by angle ϕ

ψ = angle between the surface normal and the normal to the crystallographic planes from which an x-ray peak is diffracted

σ_1, σ_2 = principal stresses on the surface.

This equation is used to calculate the stress σ_ϕ in any direction on the surface of the specimen.

---

[1] For further information in this area, see Advances in X-Ray Analysis, published by the Proc. Annual Conf. on Applicaton of X-Ray Analysis, New York: Plenum Press, vol. 2–39, 1958–1995.

Residual stress determined from diffracted x-ray peaks represents strain averaged over a finite measurement volume comprised of the surface area irradiated by the x-ray beam and the depth to which it penetrates (typically, only a few tens of microns). When mechanical deformation processes such as grinding and shot peening produce uniform and continuous plastic strain in the materials surface layers different from that in the bulk, the resultant residual stress is referred to as a macrostress. Plastic deformation nonuniformly distributed from grain to grain in a single-phase material, or between matrix and precipitates (with dissimilar yield points) in a multiphase system, causes microresidual stresses to form. Macrostress is detected by a shift in x-ray peak position; microstress is observed through peak broadening and can be described relatively by full-width half-maximum values. The residual stress magnitudes reported herein were generated by the measurement of macrostrain at the as-processed surface, except for the armor steel thru-thickness data, which were obtained from characterization of subsurface layers after electrolytic material removal.

ARL-MD has an advanced XRD-based instrument capable of rapid, precise residual stress measurements on polycrystalline metals and ceramics. The Technology for Energy Corporation Model 1610 X-Ray Stress Analysis System features a low power x-ray source (100 w, maximum) and a fixed location linear position-sensitive proportional counter (PSPC) and employs the $\sin^2\psi$ stress-measuring technique. The PSPC is a sealed gas detector with a 50-mm-long (2 in) carbon-coated quartz fiber wire anode for peak position encoding. At a diffractometer radius (specimen-to-detector distance) of 208.7 mm (8.2 in), the PSPC subtends approximately 12° of the instrument's diffraction angle 2θ range of 122° to 166°. Diffraction peaks in the high-back reflection region (2θ values approaching 180°) are much preferred because they show the greatest angular shift sensitivity with a given amount of stress. The Model 1610 allows for the utilization of up to 10 ψ angles per stress measurement.

The $\sin^2\psi$ technique requires a series of peak position measurements for a particular set of hkl planes be made at different tilts (ψ angles) of the crystallographic plane normal referenced to the normal of the specimen surface. The angular position of the diffracted peak is determined by least-squares parabolic curve fitting and is used to calculate d-spacing from the Bragg relation. A plot is then constructed of d-spacing vs. $\sin^2\psi$, and the slope of a least-squares line fitted to the experimental data multiplied by the x-ray elastic constant $(E/(1 + \upsilon)$ is proportional to the stress on the plane of the surface. The slope is found by differentiating Equation 1 with respect to $\sin^2\psi$:

$$\text{slope} = \left[\partial \left(d\phi\psi - d_0\right)/d_0\right] / \left[\partial \sin^2\psi\right]. \quad (2)$$

A linear d-spacing vs. $\sin^2\psi$ plot indicates that the strain distribution is homogeneous within the irradiated volume and that the assumption of a biaxial stress state is valid. Sin-square-psi plots that split into two branches (ψ-splitting) or exhibit curvature reveal a three-dimensional stress field containing pseudo-macro components of stress (average microstress within a sampled volume of grains). Additional information on the theory of XRD and the principles of XRD residual stress measurement is available from Klug and Alexander (1974), Cullity (1978), Hilley (1971), and Noyan and Cohen (1987).

2. EXPERIMENTAL PROCEDURES

All residual stress data were collected via a divergent beam, four-positive ψ angle arrangement. Other pertinent material-/process-dependent acquisition and calculation parameters are listed in Table 1. The characteristic radiation(s) and lattice planes selected for these investigations are typical for high-back reflection region residual stress characterization. The x-ray elastic constants used in calculating residual stress are bulk values taken from handbooks or literature. Bulk constants represent average elastic properties for all crystallographic directions and may be different from those experimentally determined for a particular set of planes. A brief description of each material system and the XRD residual stress analysis objective follows.

2.1 AISI 15-5PH Stainless Steel Tail Rotor Yoke. Taken from a crashed Army attack helicopter and exhibiting no physical damage, this component was analyzed for resolving the effects of in-service loading on the magnitude and uniformity of surface residual stresses introduced from shot peening. The tail rotor yoke was sent to the U.S. Army Research Laboratory - Materials Directorate (ARL-MD) from the Corpus Christi Army Depot (CCAD), Corpus Christi, TX. CCAD personnel prepared the yoke for residual stress characterization by plastic bead shot blasting the painted surface to remove the acrylic lacquer and polyamide epoxy primer, then stripping the cadmium plating with ammonium nitrate to expose the martensitic-structured base metal. Measurements were performed in the longitudinal and transverse directions at six locations: four on the nameplate face and two on the opposite face. Figure 1 is a photograph of the tail rotor yoke showing the nameplate face stress measurement locations.

Table 1. Residual Stress Acquisition and Calculation Parameters

	AISI 15-5PH Stainless Steel	MIL-A-46100C High Hardness Armor Steel	AISI 4340 Gun Tube Steel	99.5% Alumina Ceramic
Characteristic Radiation	$CrK\alpha_1$	$CrK\alpha_1$	$CrK\alpha_1$	$CrK\alpha_1$, $CuK\alpha_1$
Lattice Planes	(211)	(211)	(211)	(1 0 10), (146)
Diffraction Angle	156.1°	156.1°	156.1°	135.0°, 136.2°
Irradiated Area	1 mm × 5 mm	1 mm × 5 mm	2 mm dia.	1.5 mm × 5 mm
Elastic Constant	180 GPa	169 GPa	154 GPa	246 GPa, 289 GPa

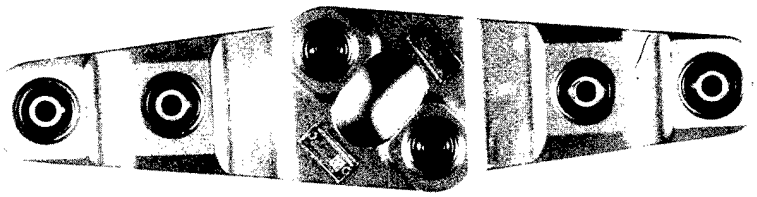

Figure 1. Army attack helicopter tail rotor yoke with nameplate face stress measurement locations 1 through 4. Locations 5 and 6 are on the opposite face.

2.2 MIL-A-46100C Armor Steel Plate. Residual stresses in light gauge, high hardness (477-534 BHN), high strength (1.36–1.44 GPa [197–207 ksi] 0.2% YS, 1.68–1.83 GPa [244–266 ksi] UTS) armor steel from quenching and tempering, cutting, grinding, and welding have been characterized for comparison to processing parameters as part of an ARL-MD exploratory development program. Surface measurements were made on as-produced quenched and tempered plate specimens for establishing baseline residual stress processing data. The measurements concentrated on the stress profiles generated at and near the free-cut edges from underwater plasma arc cutting and edge grinding operations. Magnetic particle inspection was used to confirm that the cutting and grinding did not create edge discontinuities. Plate

weldments were then fabricated per MIL-STD-1941 for the purpose of producing residual stress magnitudes and distributions on a laboratory specimen similar to those found on welded structures. Incremental subsurface residual stress analysis quantifying interior stress levels was performed on the as-produced plates and the experimental weldment after electropolishing with a 50-25-25 volumetric solution of phosphoric acid, sulfuric acid, and water.

2.3 AISI 4340 Steel Gun Tube Disk. Benet Laboratories, Watervliet, NY, requested ARL-MD measure autofrettage-produced residual stresses in a 25-mm (1.0 in)-thick disk specimen sectioned from a 120-mm gun tube for comparison to theoretical stress distribution models. In autofrettage processing, a hollow cylinder is deformed into the plastic region by applying internal pressure, causing permanent bore expansion. The resulting beneficial residual stresses increase the elastic strength of the cylinder and retard fatigue crack growth at the bore. Hoop direction measurements were made on the electropolished breech face every 2.5 mm (0.1 in) along a thru-wall I.D. to O.D. traverse.

2.4 Alumina Ceramic Block Specimens. The mechanical properties and overall performance of structural ceramic materials can be influenced by the magnitude, distribution, and depth of residual stresses effected by surface finishing operations. With the objective of using residual stress data as a method for evaluating and optimizing the grinding process, the Department of Industrial Engineering, Lehigh University, Bethlehem, PA, submitted 16 differently ground dual-channel 99.5% alumina ceramic block specimens to ARL-MD for residual stress testing services. Table 2 outlines the grinding parameters utilized for preparing the specimens. Longitudinal, or grinding direction, surface residual stresses were characterized with chromium and copper x-radiations at the center of an arbitrarily chosen channel on the nominal 102-mm × 25-mm × 19-mm (4.0 in × 1.0 in × 0.75 in) block specimens.

3. RESULTS AND DISCUSSION

3.1 AISI 15-5PH Stainless Steel Tail Rotor Yoke. The results of surface residual stress measurements in terms of location and stress-measuring direction are listed in Table 3. The data indicate that this component may have been subjected to an unusual service overload condition as was proposed as a possible explanation for cause of failure of another tail rotor yoke (Corpus Christi Army Depot 1987). Though unlikely, it is not known if the plastic media shot blast used to remove the paint caused any surface deformation. Additionally, the yoke may have been deformed at the time the aircraft crashed. For these reasons, the true shot peen-induced stress may not have been singularly characterized. However,

Table 2. Grinding Parameters for 99.5% Alumina Ceramic Block Specimens

Specimen	Wheel Bond	Mesh Size	Grit Concentration	Wheel Feed (m/s)	Cut Depth (mm)
1	Resin	80	50	2.9	1.5
2	Resin	80	50	6.9	2.6
3	Resin	80	100	2.9	2.6
4	Resin	80	100	6.9	1.5
5	Resin	180	50	2.9	2.6
6	Resin	180	50	6.9	1.5
7	Resin	180	100	2.9	1.5
8	Resin	180	100	6.9	2.6
9	Vitrified	80	50	2.9	2.6
A	Vitrified	80	50	6.9	1.5
B	Vitrified	80	100	2.9	1.5
C	Vitrified	80	100	6.9	2.6
D	Vitrified	180	50	2.9	1.5
E	Vitrified	180	50	6.9	2.6
F	Vitrified	180	100	2.9	2.6
G	Vitrified	180	100	6.9	1.5

NOTE: Grinding wheel specifications: Diamond, 178 mm diameter, 6.34 mm width, 2,400 rpm rotational speed, down cut, 22.3 m/s peripheral velocity.

two observations are noteworthy. First, the residual stresses measured at locations 1, 2, and 5, the reduced area where the failed rotor yoke fractured, are significantly lower in magnitude, especially in the longitudinal direction (major length of yoke), than those measured at other locations. The second observation is the uniformity of the measured stresses in both the longitudinal and transverse directions at locations 3, 4, and 6 (remote to the reduced areas). These values average –707 MPa (–102.6 ksi) and are in good agreement with other reported shot peening stresses (Wohlfahrt 1982).

Table 3. Residual Stress Measurement Results From Shot-Peened Army Attack Helicopter Tail Rotor Yoke

Location	Residual Stress	
	Longitudinal Direction (MPa [ksi])	Transverse Direction (MPa [ksi])
1	–223 (–32.4)	–477 (–64.8)
2	–298 (–43.2)	–445 (–64.5)
3	–788 (–112.9)	–694 (–100.6)
4	–674 (–97.8)	–761 (–110.4)
5	–168 (–24.3)	–444 (–64.4)
6	–622 (–90.2)	–714 (–103.5)

NOTE: Negative sign indicates compressive stress.

3.2 MIL-A-46100C Armor Steel Plate. The residual stress data from an as-produced (spray-water roller quenched, tempered at 400° F/~50 min) armor plate are presented in Figure 2. Compressive stresses were measured at all surface locations along a traverse starting at the plasma cut and ground edge. However, at and near the edge, the stresses were less compressive in magnitude than those remote to the edge, indicating that the cutting and grinding processes altered the as-produced residual stress state. Subsurface residual stress profiles were compressive to a depth of roughly 0.25 mm (0.010 in), then became tensive and remained so for the balance of the 0.58-mm (0.023 in)-deep thru-thickness characterization. Microstructural examination of the as-produced plates had revealed the existence of an approximately 0.13-mm (0.005 in)-thick decarburized surface layer. Consistent with reported effects of decarburization (Hilley 1971), the measured residual compressive stresses decreased toward the surface. Figure 3 displays residual stresses measured in the transverse direction (perpendicular to the weld line) at the surface of the butt-welded plate specimen along with those measured at the same locations prior to welding. The distance offset in the start of the "after welding" trace is equal to half the width of the weld bead. Examination of Figure 3 reveals a steep stress gradient in the heat-affected zone (HAZ) with the residual welding stress values and distribution in general agreement with predicted restrained butt-weld stress data (Masubuchi 1980). Results from subsurface measurements parallel to the weld show tensive stresses in the HAZ approaching 50% of yield strength at 0.13 mm (0.005 in) below the surface. At the 0.46 mm (0.018 in) depth, the stress magnitudes increase to 70% of yield.

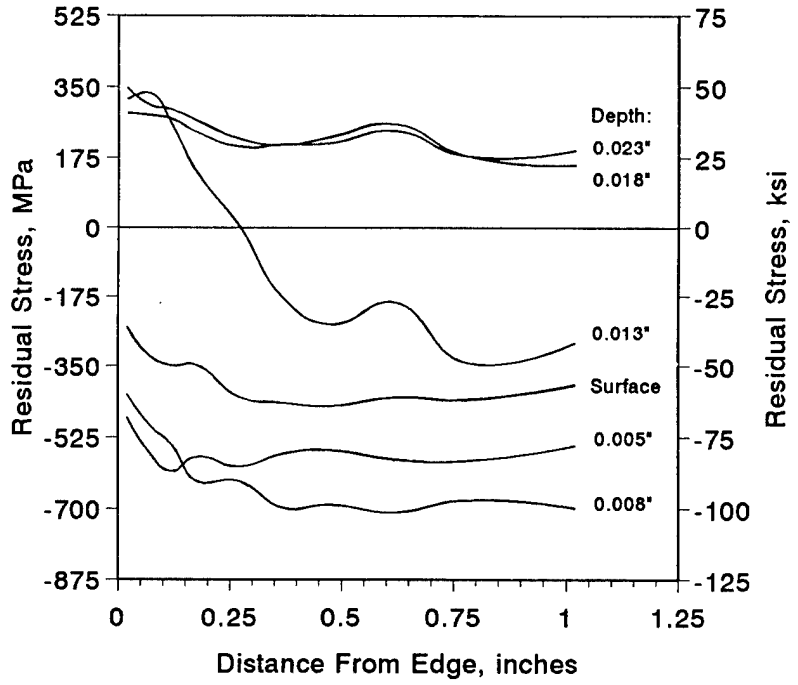

Figure 2. Surface and thru-thickness residual stress on as-produced high hardness armor steel plate.

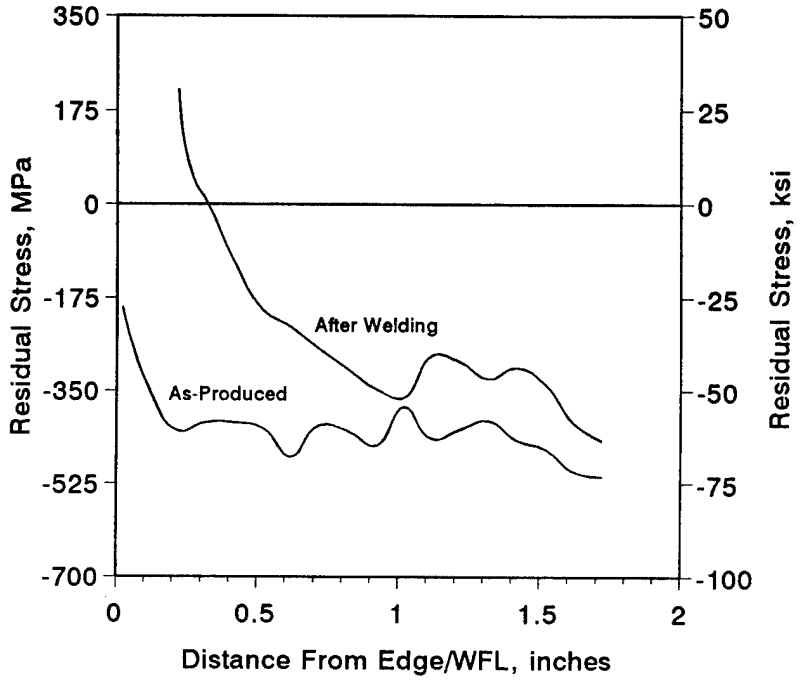

Figure 3. As-produced and after welding surface residual stress on high hardness armor steel plate.

3.3 AISI 4340 Steel Gun Tube Disk. Figure 4 shows the graph of percent deviation between gun tube disk predicted (from a two-dimensional, nonlinear elastic-plastic finite element analysis model) and measured residual hoop stresses. Between the 0.14-in and 0.94-in traverse locations, the agreement is excellent—within 4.65%. From 1.04 in to 2.04 in, it is noticed that a slightly increasing percent deviation was obtained indicating a possible relief of residual stress upon cutting the disk from the gun tube. The larger excursions, such as at the 1.04-in, 1.64-in, and 2.14-in locations, could be attributed to surface preparation irregularities. Whereas, at the I.D. and O.D. (0.04-in and 2.24-in locations, respectively), the deviations may be due to the "rounding off" of the free edges during electropolishing causing an error in true ψ-position.

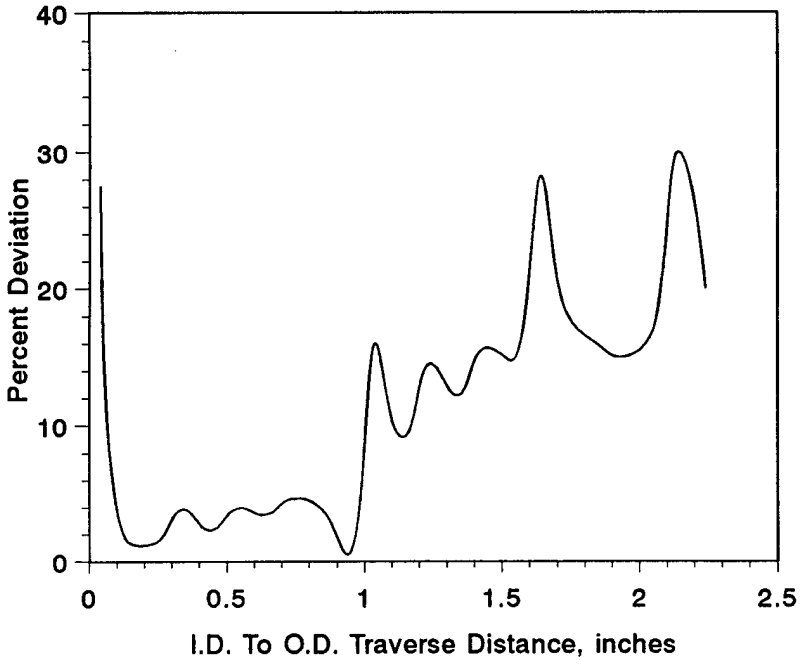

Figure 4. Percent deviation between gun tube disk predicted and measured residual stress.

3.4 Alumina Ceramic Block Specimens. Table 4 lists grinding direction residual stress measurement results. Employing both chromium and copper x-radiations for this study allowed for the determination of residual stress at two surface layer depths. The copper radiation penetrated approximately three times deeper due to the threefold difference in the linear absorption coefficient of the alumina for these radiations (μ_{Cr} = 794 vs. μ_{Cu} = 264). Lange, James, and Green (1983) have reported the depths of penetration in hot-pressed alumina (1,500° C/2 hr) for 50% diffracted intensity from chromium and copper

Table 4. Grinding Direction Residual Stress Measurement Results From 99.5% Alumina Ceramic Block Specimens

Specimen	Residual Stress	
	CrK_α Radiation (MPa [ksi])	CuK_α Radiation (MPa [ksi])
1	−104 (−15.1)	231 (33.5)
2	−253 (−36.7)	187 (27.1)
3	−120 (−17.4)	292 (42.3)
4	−223 (−32.3)	276 (40.1)
5	−70 (−10.1)	261 (37.8)
6	−131 (−19.0)	234 (33.9)
7	−165 (−24.0)	230 (33.4)
8	−94 (−13.7)	214 (31.0)
9	−86 (−12.5)	216 (31.3)
A	−181 (−26.3)	214 (31.1)
B	−191 (−27.7)	260 (37.7)
C	−242 (−35.1)	248 (36.0)
D	−114 (−16.5)	226 (32.8)
E	−109 (−15.8)	237 (34.4)
F	−85 (−12.3)	247 (53.8)
G	−36 (−5.2)	263 (38.2)

NOTE: Negative sign indicates compressive stress.

radiations as 8 μm and 26 μm, respectively. The variation in the chromium radiation residual stress data, which ranges from −36 MPa to −253 MPa (−5.2 ksi to −36.7 ksi) and averages −138 MPA ±64 MPa (−20.0 ksi ±9.3 ksi), suggests that the magnitude of the compressive stress may be a function of the grinding condition. This is not apparent from the copper radiation results as a relatively uniform tensive stress, averaging 240 MPa ±27 MPa (34.8 ksi ±3.9 ksi), was measured on all specimens. The crossover from compressive to tensive residual stress occurs at a depth of approximately 5–10 μm, indicating that the grinding-induced plastic deformation exists in a shallow surface layer.

4. SUMMARY

The x-ray diffraction residual stress analysis applications presented herein demonstrate the usefulness and versatility of this technique for characterizing process-induced residual stress in U.S. Army and other material systems.

5. REFERENCES

ASM International. "Practical Applications of Residual Stress Technology." Proc. 3rd Intl. Conference, Materials Parks, OH, 1991.

Hilley, M. E. (ed.). "Residual Stress Measurement by X-Ray Diffraction - SAE J784a." Soc. of Auto. Eng., Warrendale, PA, 1971.

Kula, E., and V. Veiss (eds.). "Residual Stress and Stress Relaxation." Proc. 28th Sagamore Army Material Research Conference, New York: Plenum Press, 1982.

Hauk, V., H. Hougardy, and E. Macherauch (eds.). "Residual Stresses: Measurement, Calculation, Evaluation." Proc. Conf. on Residual Stresses, DGM Informationsgesellschaft, Verlag, Oberursel, 1991.

Corpus Christi Army Depot. CCAD Report No. 88MX022, Corpus Christi, TX, November 1987.

Cullity, B. D. Elements of X-Ray Diffraction, Addison-Wesley, second edition, Reading, MA, 1978.

Klug, H. P., and L. E. Alexander. X-Ray Diffraction Procedures, second edition, New York: John Wiley and Sons, 1974.

Lange, F. F., M. R. James, and D. J. Green. "Determination of Residual Stresses Caused by Grinding in Polycrystalline Al_2O_3." Journal of American Ceramic Society, vol. 66, no. 2, chap. 16–17, 1983.

Masubuchi, K. Analysis of Welded Structures, Elmsford, NY: Pergamon Press, first edition, p. 198, 1980.

Noyan, I. C., and J. B. Cohen. Residual Stress: Measurement by Diffraction and Interpretation, New York: Springer-Verlag, 1987.

Wohlfahrt, H. "Shot Peening and Residual Stresses." Proc. 28th Sagamore Army Material Research Conference, New York: Plenum Press, 1982.

NO. OF COPIES	ORGANIZATION
2	DEFENSE TECHNICAL INFO CTR ATTN DTIC DDA 8725 JOHN J KINGMAN RD STE 0944 FT BELVOIR VA 22060-6218
1	DIRECTOR US ARMY RESEARCH LAB ATTN AMSRL OP SD TA 2800 POWDER MILL RD ADELPHI MD 20783-1145
3	DIRECTOR US ARMY RESEARCH LAB ATTN AMSRL OP SD TL 2800 POWDER MILL RD ADELPHI MD 20783-1145
1	DIRECTOR US ARMY RESEARCH LAB ATTN AMSRL OP SD TP 2800 POWDER MILL RD ADELPHI MD 20783-1145
	ABERDEEN PROVING GROUND
2	DIR USARL ATTN AMSRL OP AP L (305)

NO. OF COPIES	ORGANIZATION
1	ASST SEC OF THE ARMY RESEARCH AND DEVELOPMENT ATTN DEPT FOR SCI & TECH THE PENTAGON WASHINGTON DC 20310-0103
1	COMMANDER US ARMY ARDEC ATTN AMSTA AR IMI I STINFO BLDG 59 PICATINNY ARSENAL NJ 07806-5000
1	COMMANDER ROCK ISLAND ARSENAL ATTN SMCRI ENM ROCK ISLAND IL 61299-5000
1	MIAC CINDAS PURDUE UNIVERSITY PO BOX 2634 WEST LAFAYETTE IN 47906
1	COMMANDER US ARMY TANK AUTOMOTIVE R&D COMMAND ATTN AMSTA DDL TECH LIB WARREN MI 48397-5000
1	COMMANDANT US MILITARY ACADEMY ATTN DEPT OF MECHANICS WEST POINT NY 10966-1792
1	US ARMY MISSILE COMMAND REDSTONE SCI INFO CENTER ATTN DOCS SEC BLDG 4484 REDSTONE ARSENAL AL 35898-5241
1	COMMANDER US ARMY NGIC ATTN DRXST SD 220 7TH ST NE CHARLOTTESVILLE VA 22901
1	COMMANDER US ARMY LABCOM ISA ATTN SLCIS IM TL 2800 POWDER MILL RD ADELPHI MD 20783-1145

NO. OF COPIES	ORGANIZATION
1	COMMANDER US ARMY RESEARCH OFC ATTN CHIEF IPO PO BOX 12211 RESEARCH TRIANGLE PARK NC 27709-2211
1	DIRECTOR US NAVAL RSRCH LAB ATTN MATLS SCI & TECH DIV CODE 26 27 DOC LIBRARY WASHINGTON DC 20375
1	DIRECTOR BENET LABORATORIES CCAC ATTN AMSTA AR CCB TL WATERVLIET NY 12189-4050
1	COMMANDER US ARMY NRDEC ATTN SATNC MI TECHNICAL LIBRARY NATICK MA 01760-5010
1	WRIGHT LAB TECH LIBRARY WL DOC BLDG 22 AREA B WP AFB OH 45433
1	NASA LANGLEY RESEARCH CTR TECHNICAL LIBRARY MAIL STOP 185 BLDG 1194 HAMPTON VA 23681-0001
1	NASA WHITE SANDS TECH LIBRARY ATTN STEWS IM ST LAS CRUCES NM 88002
1	LOS ALAMOS NATL LAB LIBRARY MS P362 PO BOX 1663 LOS ALAMOS NM 87545-0020
1	COMMANDER AIR FORCE ARMAMENT LAB ATTN AFATL MN EGLIN AFB FL 32542-5434

NO. OF COPIES	ORGANIZATION
1	SANDIA NATIONAL LABS TECHNICAL LIBRARY DEPT 3140 PO BOX 5800 ALBUQUERQUE NM 87185
1	NIST OFC OF INFO SERVICES RSRCH INFO CENTER ADMIN BLDG E106 GAITHERSBURG MD 20899
1	COLD REGIONS RESEARCH & ENGRNG LAB LIBRARY 72 LYME RD HANOVER NH 03755-1290
1	MARTIN MARIETTA ENRGY SYS CENTRAL RESEARCH LIB ORNL PO BOX 2008 OAK RIDGE TN 37831-6208
1	PENN STATE UNIVERSITY APPLIED RSRCH LAB LIBRARY PO BOX 30 STATE COLLEGE PA 16804-0030
1	MASSACHUSETTS INSTITUTE OF TECHNOLOGY BARKER ENGINEERING LIB RM 10 500 BOSTON MA 02139
1	TECHNOLOGY FOR ENRGY CORP 10737 LEXINGTON DR PO BOX 22996 KNOXVILLE TN 37933-0996
1	LAMBDA RESEARCH 5521 FAIR LANE CINCINNATI OH 45227
1	SOUTHWEST RSRCH INSTITUTE NONDESTRUCTIVE TESTING INFO ANALYSIS CENTER 6220 CULEBRA RD POD 28510 SAN ANTONIO TX 78284

NO. OF COPIES	ORGANIZATION
	ABERDEEN PROVING GROUND
15	DIR, USARL ATTN: AMSRL-MA-I, D. SNOHA

NO. OF COPIES	ORGANIZATION
1	PROTO MANUFACTURING LTD 2175 SOLAR CIRCLE OLDCASTE ONTARIO NOR1L0 CANADA

USER EVALUATION SHEET/CHANGE OF ADDRESS

This Laboratory undertakes a continuing effort to improve the quality of the reports it publishes. Your comments/answers to the items/questions below will aid us in our efforts.

1. ARL Report Number/Author ARL-TR-1024 (Snoha) Date of Report September 1996

2. Date Report Received _____

3. Does this report satisfy a need? (Comment on purpose, related project, or other area of interest for which the report will be used.) _____

4. Specifically, how is the report being used? (Information source, design data, procedure, source of ideas, etc.) _____

5. Has the information in this report led to any quantitative savings as far as man-hours or dollars saved, operating costs avoided, or efficiencies achieved, etc? If so, please elaborate. _____

6. General Comments. What do you think should be changed to improve future reports? (Indicate changes to organization, technical content, format, etc.) _____

CURRENT ADDRESS

_____
Organization

_____
Name

_____
Street or P.O. Box No.

_____
City, State, Zip Code

7. If indicating a Change of Address or Address Correction, please provide the Current or Correct address above and the Old or Incorrect address below.

OLD ADDRESS

_____
Organization

_____
Name

_____
Street or P.O. Box No.

_____
City, State, Zip Code

(Remove this sheet, fold as indicated, tape closed, and mail.)

(DO NOT STAPLE)